

## ORIGINAL ARTICLE

# Frataxin deficiency alters gene expression in Friedreich ataxia derived iPSC-neurons and cardiomyocytes

Mariana B. Angulo<sup>1,2</sup>  | Alexander Bertalovitz<sup>1,3</sup> | Mariana A. Argenziano<sup>1</sup> | Jiajia Yang<sup>1,2</sup> | Aarti Patel<sup>3</sup> | Theresa Zesiewicz<sup>4</sup> | Thomas V. McDonald<sup>1,2,3</sup> 

<sup>1</sup>Heart Institute, Morsani College of Medicine, University of South Florida, Tampa, Florida, USA

<sup>2</sup>Department of Molecular Pharmacology & Physiology, Morsani College of Medicine, University of South Florida, Tampa, Florida, USA

<sup>3</sup>Department of Medicine (Cardiology), Morsani College of Medicine, University of South Florida, Tampa, Florida, USA

<sup>4</sup>Department of Neurology, Morsani College of Medicine, University of South Florida, Tampa, Florida, USA

## Correspondence

Thomas V. McDonald, USF Heart Institute, 560 Channelside Drive, Tampa, FL 33602, USA.  
Email: [thomasmcdonald@usf.edu](mailto:thomasmcdonald@usf.edu)

## Funding information

University of South Florida-Preeminence Fund

## Abstract

**Background:** Friedreich's ataxia (FRDA) is an autosomal recessive disease, whereby homozygous inheritance of an expanded GAA trinucleotide repeat expansion in the first intron of the *FXN* gene leads to transcriptional repression of the encoded protein frataxin. FRDA is a progressive neurodegenerative disorder, but the primary cause of death is heart disease which occurs in 60% of the patients. Several functions of frataxin have been proposed, but none of them fully explain why its deficiency causes the FRDA phenotypes nor why the most affected cell types are neurons and cardiomyocytes.

**Methods:** To investigate, we generated iPSC-derived neurons (iNs) and cardiomyocytes (iCMs) from an FRDA patient and upregulated *FXN* expression via lentivirus without altering genomic GAA repeats at the *FXN* locus.

**Results:** RNA-seq and differential gene expression enrichment analyses demonstrated that frataxin deficiency affected the expression of glycolytic pathway genes in neurons and extracellular matrix pathway genes in cardiomyocytes. Genes in these pathways were differentially expressed when compared to a control and restored to control levels when FRDA cells were supplemented with frataxin.

**Conclusions:** These results offer novel insight into specific roles of frataxin deficiency pathogenesis in neurons and cardiomyocytes.

## KEYWORDS

extracellular matrix, frataxin, Friedreich's ataxia, glycolysis, lentivirus

## 1 | INTRODUCTION

Friedreich's ataxia (FRDA) is an autosomal recessive neurodegenerative disease with a progressive course. Most cases are caused by a GAA trinucleotide repeat expansion (above 66 repeats in the first intron of the frataxin gene (*FXN*, OMIM:606829)), resulting in transcriptional repression of

frataxin (Campuzano et al., 1996; Campuzano et al., 1997; Cossee et al., 1997). FRDA is the most common inherited ataxia, with a prevalence of 1 in 50,000 Caucasians and a carrier frequency of 1:60 to 1:100 (Campuzano et al., 1996; Cossee et al., 1997; Delatycki et al., 2000). Neurological symptoms typically appear in the first decade of life due to sensory neuron degeneration in the dorsal root ganglia,

This is an open access article under the terms of the [Creative Commons Attribution-NonCommercial-NoDerivs](https://creativecommons.org/licenses/by-nc-nd/4.0/) License, which permits use and distribution in any medium, provided the original work is properly cited, the use is non-commercial and no modifications or adaptations are made.

© 2022 The Authors. *Molecular Genetics & Genomic Medicine* published by Wiley Periodicals LLC.

the cerebellar, and the spinocerebellar tracts (De Biase et al., 2007; Koeppen & Mazurkiewicz, 2013). Neuronal degeneration leads to loss of balance and coordination, sensory loss, muscle weakness, and dysarthria (Koeppen & Mazurkiewicz, 2013).

FRDA is considered a multisystem disorder; however, that impacts the central and peripheral nervous systems, the musculoskeletal system, the heart, and the pancreas (Keita et al., 2022). Common musculoskeletal features include scoliosis, pes cavus, and talipes equinovarus. About half of the FRDA patients display glucose intolerance, and studies have found that diabetes mellitus is more prevalent in these patients, with estimates between 1% and 32% (Cnop et al., 2012; Finocchiaro et al., 1988; Gucev et al., 2009; Isaacs et al., 2016).

Approximately 60% of the patients with FRDA develop progressive cardiac disease that appears similar to primary hypertrophic cardiomyopathy (HCM) but is characterized by more progressive cardiac fibrosis, systolic dysfunction, and arrhythmias (Gunal et al., 1996; Harding & Hewer, 1983; Kawai et al., 2000). In most cases, the electrocardiogram (ECG) displays repolarization abnormalities that come in the form of T-wave inversion or flattening in lateral or inferior leads and ST-segment elevation or depression. Typical echocardiographic findings involve increased end-diastolic septal and posterior wall thicknesses and left ventricular hypertrophy. 20% of FRDA patients present reduced ejection fraction in the second to third decade of life, usually after the neurological disease is well established (Koeppen et al., 2015; Pousset et al., 2015). Cardiac involvement in FRDA patients is variable however and has been reported in some instances to precede neurological dysfunction, while in other cases, cardiac disease is never manifest (Hanson et al., 2019; Zesiewicz et al., 2020). This unpredictable discordance between neurological and cardiac disease onset suggests different pathophysiological mechanisms and cell-type susceptibility to GAA repeat expansion and frataxin deficiency.

There are multiple proposed functions of frataxin including involvement in iron homeostasis, cellular redox reaction regulation, iron–sulfur cluster biogenesis, and heme synthesis (Adamec et al., 2000; Adinolfi et al., 2009; Becker et al., 2002; Yoon & Cowan, 2003, 2004). However, none of them fully explain why its deficiency generates the various FRDA phenotypes. Among the possibilities are that frataxin may play different roles in neurons and cardiomyocytes and that the GAA expansion itself may have a pathological role independent of frataxin (Al-Mahdawi et al., 2008; Castaldo et al., 2008). It is also unclear why deficiency of ubiquitously expressed frataxin selectively affects neurons and myocardium (Koutnikova et al., 1997).

Presently, there is no approved effective therapy to prevent or reverse FRDA pathology (Aranca et al., 2016;

Zesiewicz et al., 2020). Therefore, generating reliable cellular models that recapitulate FRDA-related molecular processes is important for studying disease mechanisms, and identification of therapeutic targets and disease biomarkers (Hick et al., 2013). Cells derived from FRDA patients are a relevant cell model as they carry the complete *FXN* locus with the GAA expansion and regulatory sequences. Since intact neurons and cardiomyocytes are not routinely accessible from patients, the ability to differentiate human induced pluripotent stem cells (iPSCs) into iNs and iCMs to generate model systems derived from patient cells that closely mimic the disease is crucial for FRDA. Here, we generated iPSCs from peripheral blood mononuclear cells (PBMCs) derived from an FRDA patient to study iNs and iCMs. Since FRDA is a progressive disease, taking years to manifest, by studying newly differentiated neurons and cardiomyocytes (with and without re-introducing frataxin), we biased towards early molecular processes in frataxin deficiency, independent of the GAA expansion. Our results suggest that frataxin absence may specifically affect glycolysis in neurons and the extracellular matrix in cardiomyocytes. These findings provide insights into possible pathological differences between the two tissues in FRDA.

## 2 | METHODS

### 2.1 | Ethical compliance

Written informed consent was obtained from the patient. The study was approved by the Institutional Review Board of the University of South Florida (IRB: Pro00033948) and was conducted according to the Principles of the Declaration of Helsinki.

### 2.2 | Cell reprogramming and iPSC culture

We recruited a 34-year-old male with FRDA through the Friedreich Ataxia Neurology Clinic at the University of South Florida, Morsani College of Medicine. Clinical information about the subject is provided in Table 1. PBMCs from the FRDA subject were reprogrammed into iPSCs using the CytoTune™-iPS 2.0 Sendai Reprogramming Kit (A16517, Thermo Fisher). The iPSCs were cultured in mTESR plus medium (100–0276, STEMCELL Technologies) on Matrigel-coated plates (354277) and passaged every time they reached 60% confluency using EDTA 0.5 mM. They were maintained at 37°C, 5% CO<sub>2</sub>, and 85% relative humidity, and the medium was changed every other day. The control

TABLE 1 Patient clinical information

Gender	Age	Ethnicity	GAA expansion	First neurological symptom	Age of onset neurological symptom	Neurological status at enrollment	First cardiac symptom	Age of onset cardiac symptom	ECG	Other symptoms
Male	34 years	Caucasian	1092 & 781	Difficulty walking	8	Wheelchair-bound, slurred speech, lack of coordination, Balance problem	Chest pain	28	TWI	Scoliosis, kyphoscoliosis, Osteoarthritis of spine

Abbreviation: TWI, T wave inversions.

cell line was purchased from ATCC (ACS-1026, from a Caucasian male) and cultured as described above. The FRDA-iPSC characterization and validation of the pathogenic GAA trinucleotide were previously described (Angulo et al., 2021).

### 2.3 | Neuron differentiation

For neuron differentiation, we used a Gibco media system (Figure 1a). For neural induction, iPSCs were seeded to reach 15%–20% confluency on Matrigel-coated plates after 1 day of splitting them. mTESR plus medium was exchanged at this confluency for a pre-warmed neural induction medium (A1647801, Thermo Fisher). This medium was replaced every 2 days until day 7. By day-7, the iPSCs have differentiated into Neural Stem Cells (NSCs). NSCs were dissociated with StemPro Accutase (A1110501, Thermo Fisher), expanded using neural expansion medium (A1647801 + 12634010, Thermo Fisher), and characterized before further differentiation (Figure 1b–e). After expanding NSCs to passage 1, they were dissociated and seeded on Matrigel-coated plates with neural differentiation medium (A3653401, Thermo Fisher) to achieve neuron differentiation. This medium was replaced every 2 days. Neurons were observed 7 days after neuron media was added. Their characterization is shown in Figure 1c–e.

### 2.4 | Cardiomyocyte differentiation

iPSCs derived from the FRDA subject and control were differentiated into iCMs with the STEMdiff™ Cardiomyocyte Differentiation Kit (# 05010, STEMCELL Technologies) per manufacturer's protocol (Figure 2a). Briefly, iPSCs were seeded on Matrigel-coated plates with mTESR plus medium until they reached ~95% confluency. Then, the medium was changed to STEMdiff™ Cardiomyocyte Differentiation Medium A with matrigel (1:100) for 2 days, followed by STEMdiff™ Cardiomyocyte Differentiation Medium B for 2 days, and STEMdiff™ Cardiomyocyte Differentiation Medium C for 4 days. They were subsequently maintained in STEMdiff™ Cardiomyocyte Maintenance Medium, and the medium was changed every other day. iCMs were purified with a metabolic-selection method using glucose starvation (RPMI-glucose + B27) (11879020, 17504044, Thermo Fisher) for 5 days as previously described (PMID: 25867738). For downstream experiments, iCMs were dissociated with cardiomyocyte dissociation media (# 05025, STEMCELL Technologies). iCM characterization is shown in Figure 2b–d.

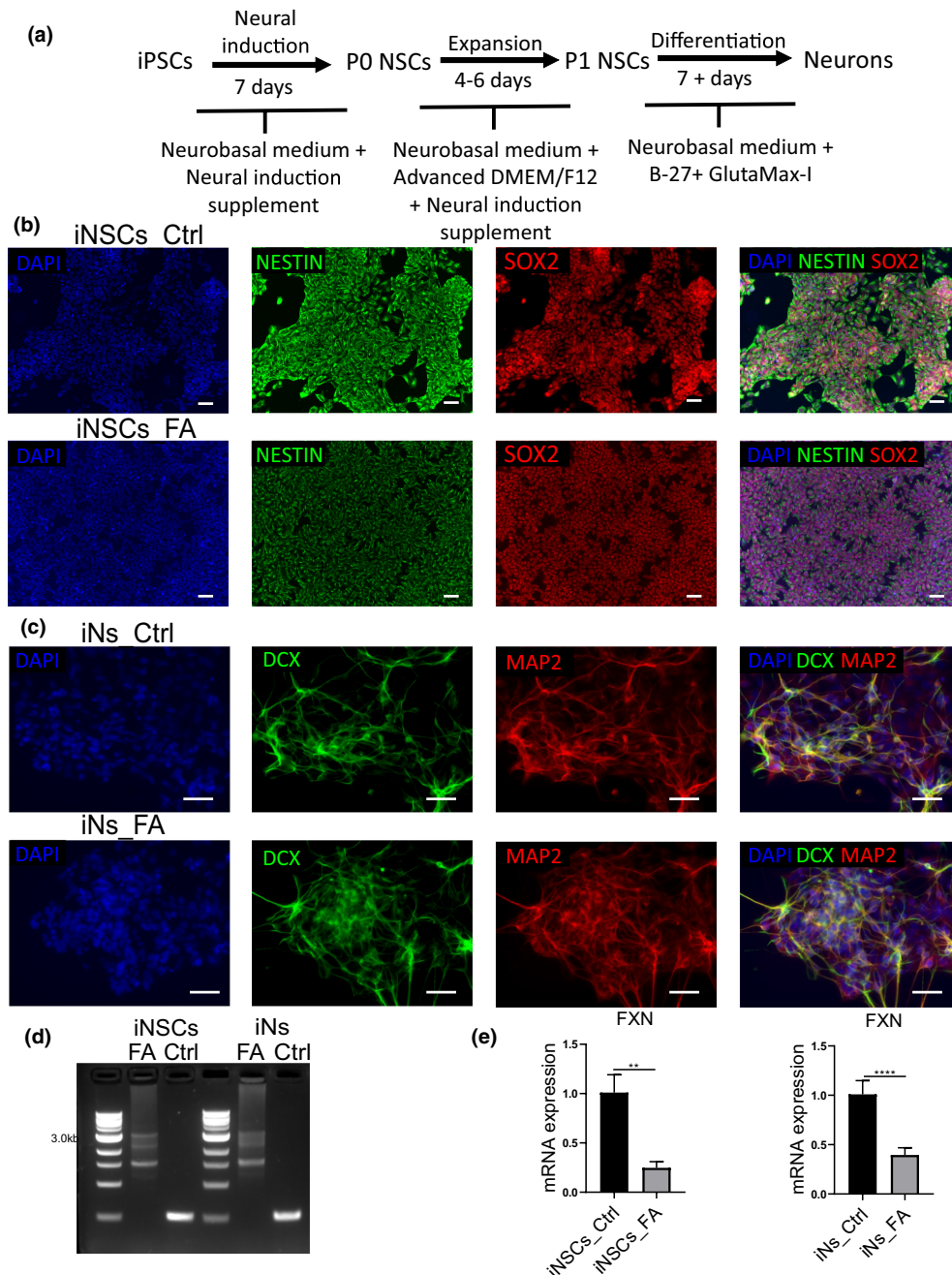


**FIGURE 1** iNSCs and iNs characterization. (a) Protocol diagram for neuron differentiation. (b) Immunostaining of control and patient iPSC-derived neural stem cells (iNSCs) showed expression of the markers NESTIN (green) and SOX2 (red). Nuclei were stained with DAPI (blue). Scale bar 50  $\mu$ m. (c) Immunostaining of control and patient iNs showing expression of neuron markers of DCX (green) and MAP2 (red). Nuclei were stained with DAPI (blue). Scale bar 50  $\mu$ m. (d) PCR analysis of the GAA repeat region in the *FXN* gene using genomic DNA extracted from iNSCs and iNs from control and FRDA patient. (e) qPCR quantification of *FXN* mRNA levels in iNSCs and iNs from control and FRDA patient. Data are expressed as means  $\pm$  SD of three independent experiments. \* $p$  < 0.05. \*FA means FRDA.

## 2.5 | Immunofluorescence analysis

Cells were fixed in 4% PFA (28,908, Thermo Fisher) for 15 min at room temperature, permeabilized with 0.2% Triton X-100 (T8787, Sigma Aldrich) for 10 min, and

blocked for 30 min with 1% of BSA (Sigma-Aldrich) with 22.52 mg/ml glycine (BP381-500, Fisher Scientific) in PBST (phosphate-buffered saline with 0.1% Tween 20). For staining, antibodies were diluted in 1% BSA in PBST. Samples were incubated overnight at 4°C with

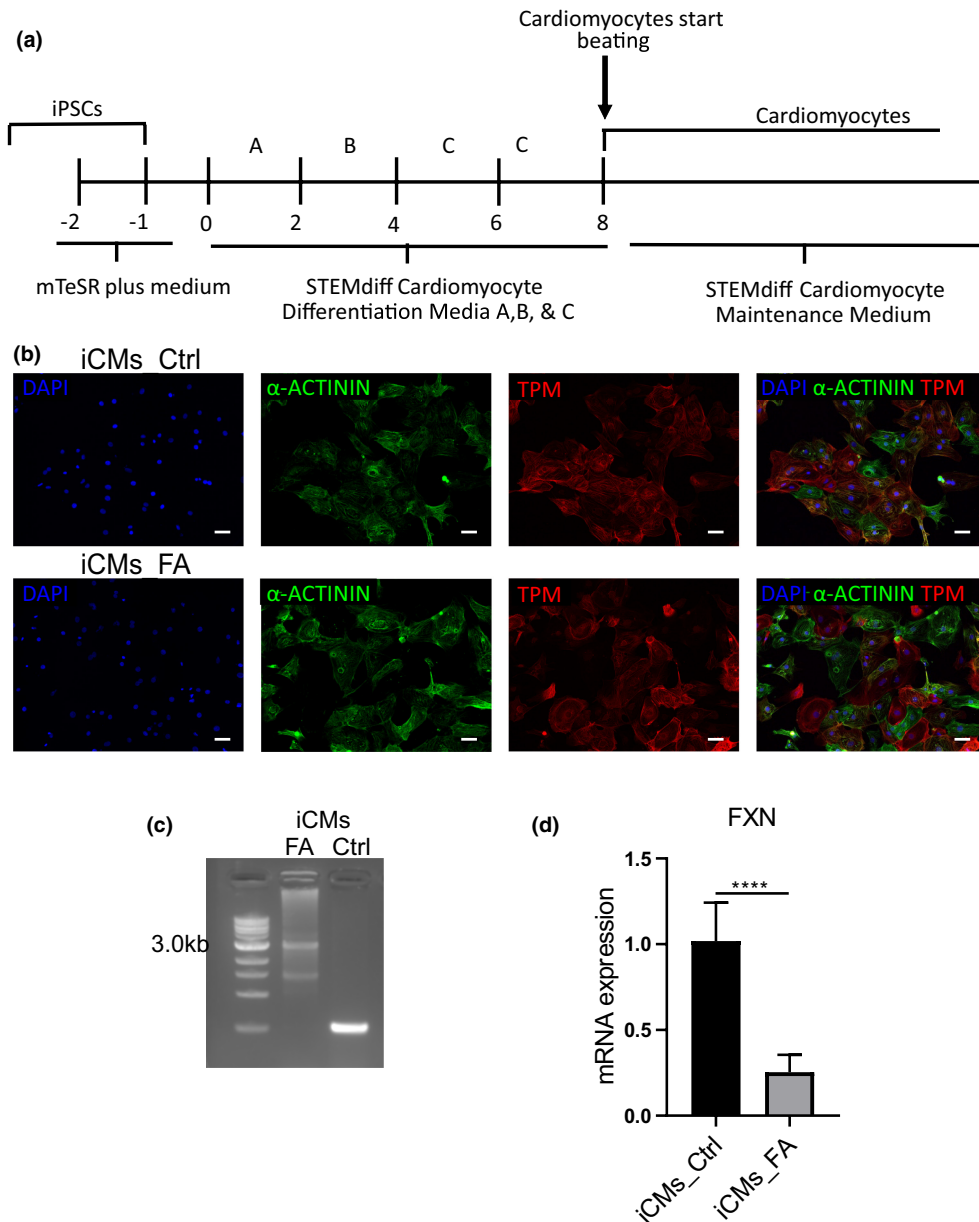


**FIGURE 2** iCMs characterization. (a) Protocol diagram for cardiomyocyte differentiation. (b) Immunostaining of control and patient iCMs showing expression markers  $\alpha$ -actinin (green) and tropomyosin (TPM) (red). Nuclei were stained with DAPI (blue). Scale bar 50  $\mu$ m. (c) PCR analysis of the GAA repeat region in the *FXN* gene using genomic DNA extracted from iCMs from control and patient. (d) qPCR quantification of *FXN* mRNA levels in iCMs from control and FRDA patient. Data are expressed as means  $\pm$  SD of three independent experiments. \* $p < 0.05$ . \*FA means FRDA.

primary antibodies. Cells were washed three times with cold PBS and incubated at room temperature for 1 h with secondary antibodies. Then they were washed three times with cold PBS, counterstained with NucBlue Reagent DAPI (R37606, Thermo Fisher), and mounted with ProLong Diamond Antifade Mountant (P36961, Thermo Fisher). Samples were imaged with a Keyence BZ-X800 fluorescence microscope and analyzed using Image J. Primary, and secondary antibodies are listed in Table S1.

## 2.6 | GAA repeat analysis

Genomic DNA from cells was isolated using the QIAamp DNA Mini and Blood Mini kit (51104, Qiagen). DNA concentration and purity were determined with the Cytation 5 reader (Agilent Technologies).

Amplification of GAA repeat expansions in the *FXN* gene was performed by PCR using primers GAA\_F: 5'-GGCTTGAACCTTCCCACACGTGTT and GAA\_R: 5'-AGGACCATCATGGCCCACTT, as previously described

(Long et al., 2017). Reactions utilized the Failsafe PCR System with mix D (FS99100). The thermal cycler was programmed as follows: 94°C for 3 min, 20 cycles of 94°C for 20s, 64°C for 30s, and 68°C for 5 min, followed by 9 cycles of 94°C for 20s, and 68° for 5 min, each subsequent elongation step increased by 15s. The last step was 68°C for 7 min. The amplification products were resolved on 1% agarose gels stained with SYBR Safe DNA Gel Stain (cat. S33102, Thermo Fisher). The length of an expanded GAA repeat was determined using the base pair size called function, of Image Lab 6.0 (BioRad). The GAA length was calculated by subtracting the length of the PCR primers and GAA flanking sequences from the number of base pairs of the PCR product and dividing the difference by three. [Number of GAA repeats = (length of base pairs of a PCR product–498)/3]The reference sequence used is NG\_008845.2.

## 2.7 | Reverse transcription and qPCR

Cells were lysed using buffer RLT (Q79216, Qiagen) and homogenized with QiaShredder (79656, Qiagen). RNA was extracted with the RNAeasy Mini Kit (74194, Qiagen). For the reverse transcription, 2 µg of RNA were mixed with 4ul of Superscript IV VILO Master Mix (# 11755050, Thermo Fisher) and DEPC water to 20µl. Samples were incubated for 10 min at 25°C, then for another 10 min at 50°C, and 5 min at 85°C. The resulting cDNA was used for qPCR.

For qPCR, cDNA was amplified on the StepOnePlus™ system (Applied Biosystems, 4376600) using TaqMan Fast Advanced Master Mix (# A44360, Thermo Fisher) and Taqman Gene expression probes *FXN* (# Hs01075496\_m1), *GAPDH* (# Hs02786624\_g1). The expression of mRNAs was normalized to the expression of glyceraldehyde 3-phosphate dehydrogenase (*GAPDH*) mRNA. Data were analyzed using the comparative Ct method (Livak & Schmittgen, 2001).

## 2.8 | Frataxin lentivirus transfer plasmid generation

The pcDNA3.1-hFrataxin-HA plasmid (31895) was obtained from Addgene. The following primers (forward) 5'-GCTCGCTAGCGCCACCATGTGGACTCTCGGGCG-3' and (reverse) 5'-GCCCGGATCCTCAAGCATCTTTTCCGGAATAGGCC-3' were synthesized (Sigma-Aldrich) and used to generate a frataxin-containing PCR product (without Human influenza hemagglutinin [HA]-tag) flanked by NHEI (5' end) and BAMHI (3' end) restrictive sites. This PCR product was digested with restriction

endonucleases NHEI and BAMHI and gel purified with the DNA Gel Extraction Kit (T1020S, NEB). The Lentiviral NanoLuc control expression vector plasmid (113450, Addgene) was obtained from Addgene and gel purified using the Monarch® DNA Gel Extraction Kit (T1020S, NEB) after being digested with restriction endonucleases NHEI and BAMHI to remove both the NanoLuc insert and the amino-terminal MYC epitope tag. T4 ligase was used to conjugate the gel-purified insert into the gel-purified backbone of the plasmid (Figure 3a). Final expression plasmids were verified by Sanger Sequencing (Eurofins Genomics).

## 2.9 | Frataxin lentivirus production

HEK293T cells were plated in Poly-d-lysine (A3890401, Thermo Fisher) coated 60 mm dishes in 5 ml media without antibiotics (RPMI-1640 supplemented with FBS, 11875093 and 16140, Thermo Fisher) so that the next day the confluency was around 70%. The day after plating, cells were transfected using the Lipofectamine 3000 transfection reagent (L3000001, Thermo Fisher) according to the manufacturer's instructions. 1.25 µg of envelope plasmid pCMV-VSV-G (8454, Addgene), 1.25 µg of packaging plasmid psPAX2 (12260, Addgene), and 2.5 µg of frataxin lentivirus transfer plasmid were used for transfection. The day after transfection, the media was replaced with 5 ml of media with antibiotics (15070063, Thermo Fisher). Two days later, the media (containing lentivirus) was collected and filtered through a 0.45 µm filter (25–245, Genesee Scientific) and stored at 4°C. 5 ml of new media with antibiotics was added to the transfected cells. Two days later, the media was collected and filtered through a 0.45 µm filter and mixed with previously collected media. Samples were aliquoted and frozen at –80°C until further analysis and transduction.

## 2.10 | Frataxin lentivirus titer and transduction

To determine the lentivirus titer, we used the Lenti-X GoStix Plus (631280 Takara), following the manufacturer's recommendations. Briefly, the GoStix Plus app was downloaded on a mobile device, and the lot number of the kit was entered. Since our lentivirus sample was unconcentrated, we tested the sample undiluted and in a 1:2 dilution to ensure a reading within the standard curve range. Following the prompts within the app, 20µl of the lentiviral supernatant (diluted and undiluted) were applied to the Lenti-X GoStix Plus cassette

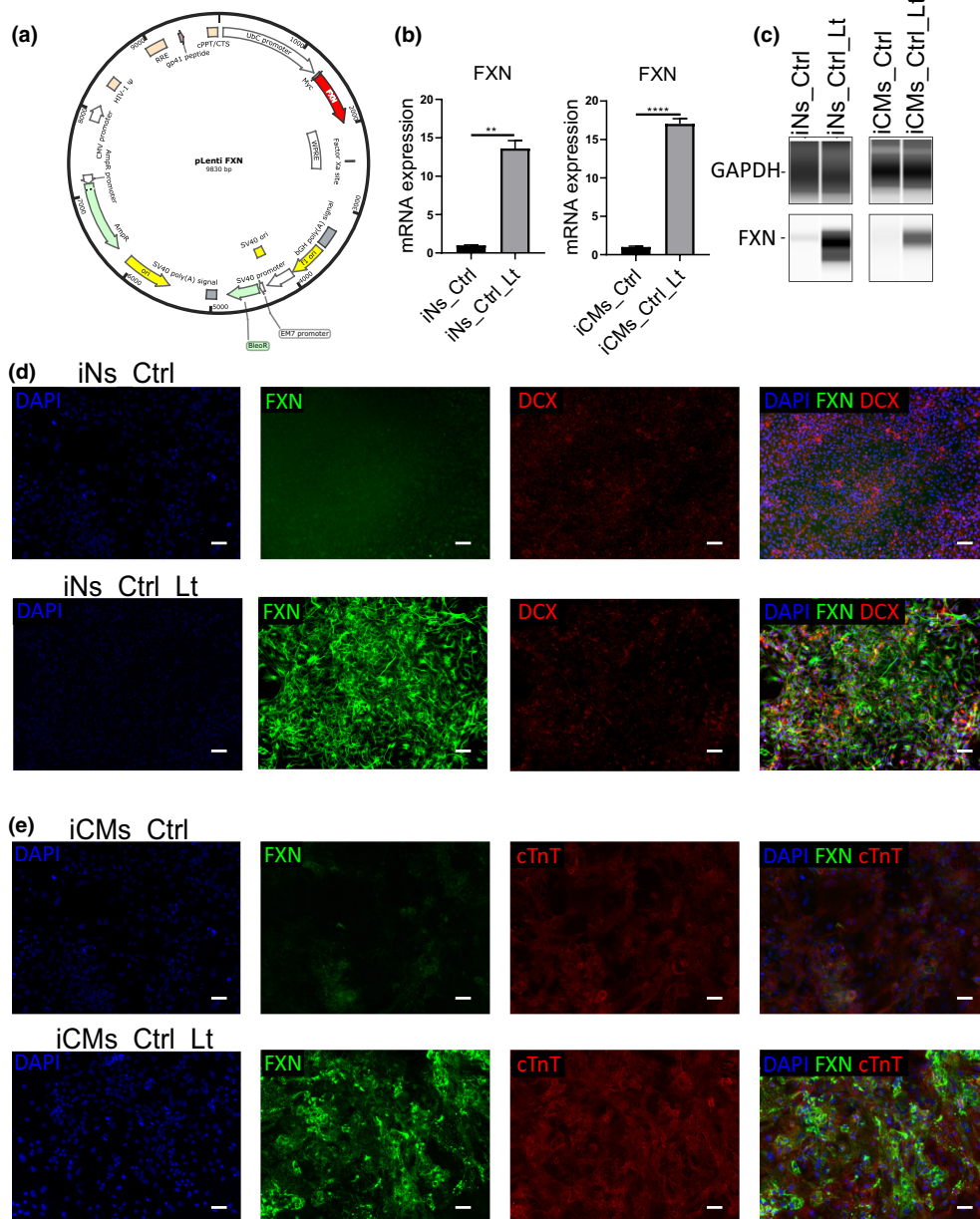


**FIGURE 3** Frataxin lentivirus validation. (a) Diagram of the modified frataxin lentiviral transfer plasmid. (b) qPCR quantification of *FXN* mRNA levels in frataxin lentivirus transduced and non-transduced control iNs and iCMs. Data are expressed as means  $\pm$  SD of three independent experiments. \* $p < 0.05$ . (c) Detection of frataxin in capillary western blot (Wes) assay in transduced and non-transduced control iNs and iCMs. (d) Immunostaining of control transduced and non-transduced iNs showing expression of FXN (green) and neuronal marker DCX (red). (e) Immunostaining of control transduced and non-transduced iCMs showing expression of FXN (green) and cardiomyocyte marker cTnT (red). \*FA means FRDA.

sample well. Then, 80  $\mu$ l of Chase Buffer were added to the sample well and allowed to appear in the cassette window. The lateral flow test was allowed to run for 10 min. Finally, the cassette was scanned with the app, which used the standard curve to calculate the titer (i.e., a GoStix Value [GV] equivalent to ng/ml p24) based on the band's intensity.

To determine the optimal concentration of lentiviral supernatant to transduce FRDA iNs and iCMs, we

assessed several dilutions of the lentivirus (Figures 4a and 5a). The cells were transduced on day 15, and the media was changed the following day to remove residual lentivirus. On day 30, iNs and iCMs were lysed, and the RNA was extracted. RT-PCR was performed to evaluate the *FXN* level compared to control and non-transduced FRDA cells. The concentration for transduction was decided based on that producing the closest *FXN* mRNA to control cells.

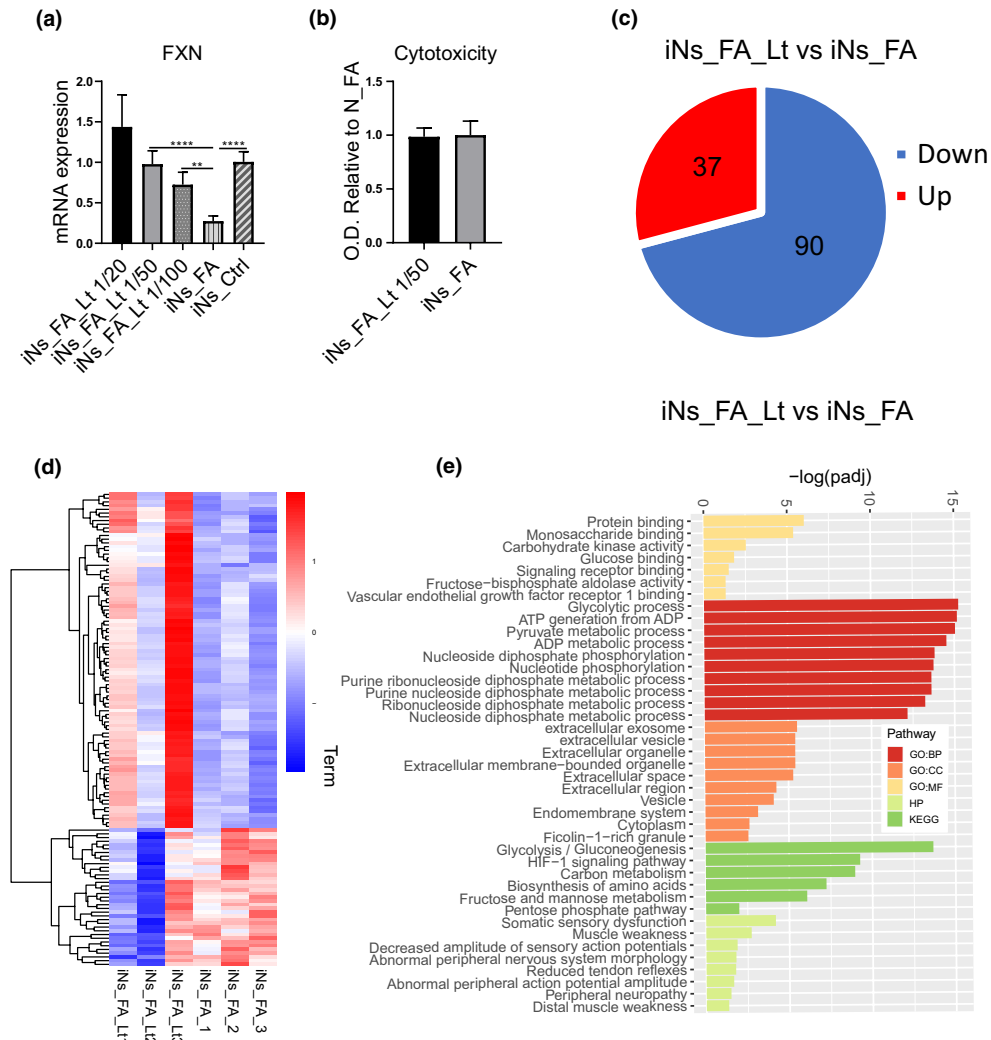


**FIGURE 4** Frataxin lentivirus transduction in FRDA iNs and RNA-seq analysis. (a) qPCR quantification of *FXN* mRNA levels of transduced FRDA iNs with different lentivirus dilutions to determine the optimal concentration for transduction (1/50 dilution equivalent to 5.4 ng/ml of p24). Data are expressed as means  $\pm$  SD of three independent experiments.  $*p < 0.05$ . (b) Cytotoxicity assay to determine if the chosen concentration for transduction was toxic to iNs. Data are expressed as means  $\pm$  SD of three independent experiments.  $*p < 0.05$ . (c) Venn diagram illustrating the differentially expressed genes between transduced and non-transduced FRDA iNs. (d) a heatmap illustrating the expression of 127 genes DE in both groups (transduced and non-transduced FRDA iNs). Three independent replicates are shown per group (e) enrichment analysis of DE genes in transduced and non-transduced iNs using g:Profiler. We included results from the gene ontology, KEGG, and human phenotype ontology databases. \*FA means FRDA.

## 2.11 | Cytotoxicity assay

To determine whether forced expression of frataxin resulted in cell toxicity we used the Cell Counting Kit-8 (CCK8) (9692, Sigma-Aldrich). 5000 cells/well (iNs and iCMs) were seeded in a 96-well plate. Cells were transduced with frataxin lentivirus, and 2 weeks later, the cytotoxicity assay was performed. 10  $\mu$ l of the CCK8 solution was added to each well of the plate containing transduced, non-transduced cells, and control without cells. After 2 h of incubation at 37°C, the absorbance was measured at 450 nm using the Cytation 5 reader (Agilent Technologies). This assay was repeated three

times, using a minimum of 6 wells per condition each time.

## 2.12 | Capillary western blot

Cells were lysed using RIPA buffer (89900, Thermo Fisher) with protease and phosphatase inhibitors (78430, Thermo Fisher). Lysates were sonicated and centrifuged for 15 min at 15,000 rpm. Protein concentration was determined with a Bradford assay (23236, Thermo Fisher). Capillary western analyses were performed using the ProteinSimple Wes<sup>®</sup> System. Samples were diluted with 0.1 $\times$  Sample



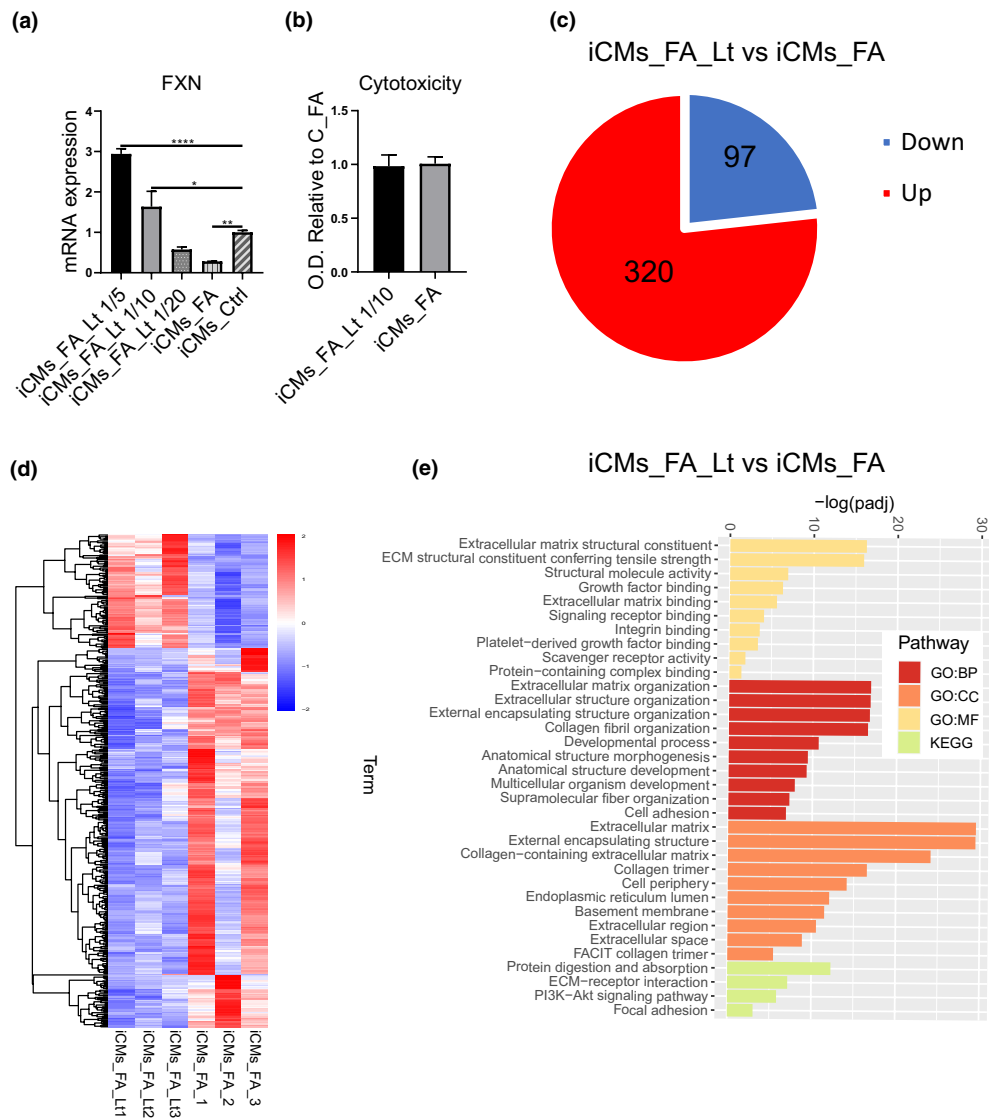


**FIGURE 5** Frataxin lentivirus transduction in FRDA iCMs and RNA-seq analysis. (a) qPCR quantification of *FXN* mRNA levels of transduced FRDA iCMs with different lentivirus dilutions to determine the optimal concentration for transduction (1/10 dilution equivalent to 27 ng/ml of p24). Data are expressed as means  $\pm$  SD of three independent experiments.  $*p < 0.05$ . (b) Cytotoxicity assay to determine if the chosen concentration for transduction was toxic to iCMs. Data are expressed as means  $\pm$  SD of three independent experiments.  $*p < 0.05$ . (c) Venn diagram illustrating the DE genes between transduced and non-transduced FRDA iCMs. (d) a heatmap illustrating the expression of 417 genes DE in both groups (transduced and non-transduced FRDA iCMs). Three independent replicates are shown per group (e) enrichment analysis of DE genes in transduced and non-transduced iCMs using g:Profiler. We included results from the gene ontology and KEGG databases. \*FA means FRDA.

Buffer. Then four parts of the diluted sample were combined with 1 part of 5 $\times$  Fluorescent Master Mix (which contains 5 $\times$  sample buffer, 5 $\times$  fluorescent standard, and 200 mM DTT) and incubated at 95°C for 5 min. After that, the samples, blocking reagent, primary, HRP-conjugated secondary antibodies, and chemiluminescent substrate were dispensed into assigned wells in a 13-well assay plate. After plate loading, the separation electrophoresis and immunodetection steps occurred in the fully automated capillary system (Protein Simple). Primary and secondary antibodies are listed in Table S1.

### 2.13 | RNA-SEQ, differential expression analysis, and enrichment analysis

RNA was isolated as described in the reverse transcription and qPCR method section. The concentration and purity of the RNA were determined with the Cytation 5 reader (Agilent Technologies). RNA from 3 biological replicates of each study group were sequenced at Novogene Co. Ltd for RNA-Seq and differential expression analysis. Briefly, 1  $\mu$ g RNA per sample was used as input material for the RNA sample preparations. Sequencing libraries

were generated using NEBNext® Ultra II TM RNA Library Prep Kit for Illumina® (E7770S, NEB) following the manufacturer's instructions, and index codes were included to assign sequences to each sample. Library quality was evaluated on the Agilent Bioanalyzer 2100 system (Agilent Technologies). Clustering the index-coded samples was performed on a cBot Cluster Generation System using PE Cluster Kit cBot-HS (PE-401-3001, Illumina). After cluster generation, the library preparations were sequenced on an Illumina platform, and paired-end reads were produced. Raw data reads of FASTQ format were processed with fastp.

Clean reads were obtained by removing reads containing adapter and poly-N sequences and low-quality reads. Q20, Q30, and GC content of the clean data were calculated. These clean reads were used for all downstream analyses. The reference genome and gene model annotation files were downloaded from genome website browser (NCBI/UCSC/Ensembl). Paired-end clean reads were aligned to the reference genome using the Spliced Transcripts Alignment to a Reference (STAR) software, and FeatureCounts was used to count the read numbers mapped of each gene. RPKM of each gene was calculated based on the length of the gene and read counts mapped to this gene. Differential expression analysis (DEA) was performed using the DESeq2 R package. The resulting *p* values were adjusted using Benjamini and Hochberg's approach to control the False Discovery Rate (FDR). Genes with an adjusted *p* < 0.05 found by DESeq2 were assigned as differentially expressed (DE). For enrichment analysis, the DE genes were submitted to g:Profiler, a web server that interprets and maps genes to the corresponding enriched pathways based on well-established data sources. We included Gene ontology, which annotates genes to biological processes, molecular functions, and cellular components; Kyoto Encyclopedia of Genes and Genomes (KEGG), which annotates genes to pathways; and Human Phenotype Ontology which provides human disease phenotype associations. Finally, Ingenuity Pathway Analysis (IPA) software (Qiagen) was used to visualize the significant networks of the most enriched pathways.

## 2.14 | Statistical analysis

Data are presented as mean ± standard deviation (SD) as indicated. Statistical significance was determined by Student's *t* test (two-tailed) for two groups and one-way ANOVA for multiple groups with post hoc test Bonferroni. Statistical significance was defined as a value of *p* < 0.05.

## 3 | RESULTS

### 3.1 | Generation of neurons and cardiomyocytes from FRDA and control iPSCs

To study the most relevant cells affected in FRDA, we generated iNs and iCMs from iPSCs derived from a FRDA subject and an unrelated control. The patient is a 34-year-old Caucasian male presenting a GAA expansion of 1092 and 781 repeats in the intron 1 of *FXN* (NG\_008845.2:g.6725GAA[(781–1092)]). He was first diagnosed with FRDA at 8-years of age due to walking difficulties. His first cardiac symptom manifested at the age of 28 with chest palpitations. At the time of enrollment in this study, he was a wheelchair user and presented several neurological, cardiac, and other symptoms typical of FRDA, summarized in Table 1. iPSCs from a control subject were purchased from the ATCC company, who was a 31-year-old Caucasian male at the time of PBMC donation. These cells have <10 GAA repeats in the *FXN* gene (Angulo et al., 2021). To differentiate the iPSCs into neurons, they were first induced into Neural Stem Cells (Figure 1a). These cells were expanded and characterized before the final differentiation into neurons. NSCs from both FRDA subject and control express the NSC markers Nestin and Sox2 (Figure 1b) and continue to divide. The GAA expansion is preserved in the FRDA subject's NSCs (Figure 1d). *FXN* mRNA level as assayed with RT-PCR demonstrates NSCs from the FRDA subject exhibited markedly reduced *FXN* than control NSCs (Figure 1e), corresponding to FRDA pathogenesis. Neuron differentiation started when NSCs were in passage 1, and fully differentiated neurons were observed at day 7 (Figure 1a). These cells expressed neuronal markers DCX and MAP2 and displayed the typical neuronal morphology of rounded cells with elongated processes connecting them (Figure 1c). The FRDA subject's neurons also preserved the GAA expansion and had significantly lower levels of *FXN* compared to those derived from the control (Figure 1d,e). iPSCs from FRDA subject and control were differentiated into iCMs and purified as described in methods until further analysis. These iCMs expressed cardiac markers α-actinin and Tropomyosin and exhibited spontaneous contractions (Figure 2b). The FRDA iCMs maintained the GAA expansion and expressed lower levels of *FXN* than control CMs (Figure 2c,d).

### 3.2 | Forced expression of frataxin in iPSC-derived neurons and cardiomyocytes

To study the role of frataxin deficiency in iPSC-derived iNs and iCMs from the FRDA-subject, we sought to restore its

expression level by transducing them with frataxin lentivirus (Figure 3a). Prior studies have found that high levels of frataxin can be toxic to cells (PMID: 29794127) (Belbellaa et al., 2020; Huichalaf et al., 2022; Vannocci et al., 2018). Therefore, we modified a transfer plasmid with a weak constitutive promoter (UbC) (113,450, Addgene) (Qin et al., 2010) to better control frataxin overexpression (Figure 3a). To test this frataxin lentivirus, we first transduced iPSC-derived iNs and iCMs from control. We harvested the cells for analysis 2 weeks post-transduction to ensure that *FXN* overexpression was not an early transient event. To evaluate the mRNA level of *FXN*, we performed RT-PCR and obtained a more than 10-fold increase in transduced Ns and CMs compared to non-transduced cells (Figure 3b). We also determined that the *FXN* mRNA was being translated into protein. Capillary western blot demonstrated an increased frataxin protein in both iNs and iCMs (Figure 3c). To verify that the overexpression of *FXN* was evenly distributed among the cells, we performed immunofluorescence staining of frataxin, co-stained with a neuron or cardiac marker (DCX and cTnT, respectively) on transduced and non-transduced iNs and iCMs. Staining showed that frataxin is overexpressed broadly in transduced iNs and iCMs (Figure 3d,e). Therefore, we concluded that transduction with this frataxin lentivirus is suitable to overexpress frataxin in iPSC-derived iNs and iCMs and can be used to complement the frataxin level in FRDA cells.

### 3.3 | Determination of frataxin lentivirus titer and optimal concentration to transduce patient's iNs and iCMs

Prior studies have shown evidence that restoring the levels of frataxin to normal levels improves phenotypes of FRDA (Chandran et al., 2017; Lim et al., 2007; Sacca et al., 2011). Prior to examining if our introduction of *FXN*-lentivirus could achieve corrective changes we ascertained that our frataxin overexpression method would result in frataxin levels in FRDA-iPSCs as close as possible to control levels. To maintain reproducibility in all the experiments, we determined the lentivirus titer using an assay quantifies the amount of p24 capsid protein present in lentiviral supernatants, which correlates directly with infectious viral titer. We obtained 270 ng/ml of p24 for the frataxin lentivirus. Then we transduced the FRDA subject iNs and iCMs with different dilutions and measured the frataxin expression with RT-PCR relative to control cells to optimize the desired amount for transduction (Figures 4a and 5a). We chose a lentivirus dilution of 1/50 (5.4 ng/ml of p24) to transduce the FRDA iNs and 1/10 (27 ng/ml of p24) to transduce the FRDA iCMs. A cytotoxicity assay

was performed to determine that this chosen amount was not toxic to iNs and iCMs. We did not observe any difference in the number of living cells between transduced and non-transduced iNs and iCMs (Figures 4b and 5b).

### 3.4 | Transcriptome profiling identifies differentially expressed genes in frataxin transduced and FRDA iPSC-derived neurons and cardiomyocytes

To identify gene expression patterns for FRDA and specifically which genes are regulated solely by frataxin levels in iNs and iCMs, we performed transcriptional profiling using RNA-seq in frataxin transduced and non-transduced cells derived from the FRDA patient. For transduced cells, RNA from 3 biological replicates was collected 2 weeks after transduction when iNs and iCMs were 30-days old (from time of differentiation). For non-transduced cells, the RNA from 3 replicates was collected on the same day, when they were 30-days old. Differential expression analysis between FRDA transduced and non-transduced cells was performed, and the genes with an adjusted  $p < 0.05$  were assigned as DE. 127 genes were DE between transduced and non-transduced FRDA-derived iNs, of which 37 were upregulated, and 90 were downregulated (Figure 4c, and Table S2). For iCMs, 417 genes were DE, 320 were upregulated with lentivirus transduction, and 97 were downregulated (Figure 5c, and Table S3). Heatmaps representing the differentially expressed genes showing the 3 replicates are shown in Figures 4d and 5d.

### 3.5 | Functional enrichment analysis of differentially expressed genes of FRDA iPSC-derived neurons and cardiomyocytes

To elucidate the potential biological function of the DE genes of iNs and iCMs derived from the FRDA subject, we performed functional enrichment analysis. The top overrepresented biological processes and pathways for iPSC-derived iNs and iCMs from the patient are shown in Figures 4e and 5e. For iPSC-derived iNs, the most significant processes were related to carbohydrate metabolism, such as Glycolysis (GO:0006096), ATP generation (GO:0006757), and ADP and Pyruvate metabolic processes (GO:0046031, GO:0006090). According to previous studies, FRDA patients have abnormal glucose metabolism and exhibit a higher risk for diabetes (Finocchiaro et al., 1988; Gucev et al., 2009; Isaacs et al., 2016; Worth et al., 2015). Additionally, lower levels of ATP that are restored with increased frataxin levels have been shown in FRDA patients and models of FRDA (Bolinches-Amoros et al., 2014;

Heidari et al., 2009; Li et al., 2015; Lodi et al., 1999). Regarding the biological pathways based on the KEGG database, Glycolysis and Gluconeogenesis (KEGG:00010) is the most significant, but HIF-1 (KEGG:04066) and Carbon metabolism (KEGG:01200) are also enriched among other related pathways. Finally, from human phenotype ontology which annotates genes to phenotypic abnormalities encountered in human disease, we obtained features of FRDA such as sensory dysfunction (HP:0003474), muscle weakness (HP:0001324), and peripheral neuropathy (HP:0009830).

From iPSC-derived iCMs, the most significantly enriched terms were related to the processes and components of the extracellular matrix, such as extracellular matrix organization (GO:0030198) and collagen fibril organization (GO:0030199). Cardiac Fibrosis, which is the consequence of extracellular matrix remodeling from pathological processes, has been observed in FRDA patients even before overt cardiac disease has developed (Hanson et al., 2019). There is also enrichment for extracellular matrix pathways, including extracellular matrix-receptor interaction (KEGG:04512) and focal adhesion (KEGG:04510).

### 3.6 | Differentially expressed genes in FRDA vs. control iPSC-derived neurons and cardiomyocytes rescued with forced frataxin expression

To further understand the role of frataxin deficiency in FRDA, we investigated the DE genes of FRDA vs. control that are restored to control levels when patient cells are transduced with frataxin. To test this, we performed RNA-seq and DEA of FRDA iPSC-iNs and iCMs compared to control iPSC-derived cells. We analyzed for the FRDA genes that were corrected to control transcription levels after frataxin lentivirus transduction. The heatmaps showing the corrected genes for both iNs and iCMs are shown in Figures 6 and 7a (Tables S2 and S3). Then, we performed functional enrichment analysis using these corrected genes to determine the overrepresented biological pathways and processes. The most significant enriched processes and pathways for iPSC-iNs are Glycolysis (KEGG:00010, GO:0006096), ATP generation (GO:0006757), and HIF-1 signaling (KEGG:04066). These were overrepresented in our previous analysis of FRDA vs. frataxin-transduced FRDA, which implicates frataxin level directly into these pathways and processes.

Similarly, for iPSC-iCMs, the enriched processes in these corrected genes are related to the extracellular matrix like in the previous analysis. This means that the frataxin deficiency is likely playing a role in these processes. IPA from the most enriched pathways for the corrected genes

in iNs and iCMs shows network diagrams with the most plausible connections to each other and genes in the IPA knowledge base (Figures 6c and 7c). For iNs, the most relevant DE genes belonging to glycolysis and gluconeogenesis included *GPI* (OMIM:172400), *HK2* (OMIM: 601125), *TPI1* (OMIM:190450), *ALDOA* (OMIM: 103850), *ENO1* (OMIM: 172430), *LDHA* (OMIM: 150000), *PFKP* (OMIM: 171840), and *PKM* (OMIM: 179050). The most relevant DE genes belonging to extracellular space in iCMs are *GDF15* (OMIM: 605312), *HMOX1* (OMIM: 141250), and *HSPG2* (OMIM: 142461).

## 4 | DISCUSSION

It is generally accepted that the loss of frataxin expression is the cause of FRDA, although there remain several unresolved questions. Despite agreement on the correlation of frataxin deficiency with FRDA, the mechanisms of disease pathogenesis, variability, and organ specificity are still not fully understood (Cook & Giunti, 2017; Delatycki & Bidichandani, 2019; Zesiewicz et al., 2020). GAA repeat expansion in FRDA is associated with altered heterochromatin and DNA methylation that correlates with the extent of the expansion, phenotype severity, and age of disease onset, possibly independent of frataxin deficiency (Al-Mahdawi et al., 2008; Castaldo et al., 2008), however study of these effects has been largely restricted to the vicinity of the *FXN* locus. Why neurons and cardiac tissue are preferentially affected in FRDA despite the ubiquitous expression of frataxin has not been resolved. Whether FRDA leads to dysfunction in nerve and heart muscle by the same or different routes is also uncertain. Here, we sought to further explore disease molecular processes by studying gene expression consequences of frataxin deficiency and interactions in relevant affected cells. Therefore, we performed transcription analysis to investigate the *FXN* network in iPSC-derived iNs and iCMs from an FRDA patient. iPSC-derived cells provide information on the early gene expression perturbations associated with frataxin-deficiency.

Restoring frataxin was associated with a change in the expression of 127 genes in iNs, primarily related to processes and pathways involved in Glycolysis, ATP generation, and HIF-1. We also found genes annotated to phenotypic abnormalities related to FRDA, such as sensory dysfunction, muscle weakness, and peripheral neuropathy such as *NDRG1*, *PLOD1*, *PLD3*, *HK1*, *HSPB8*, *SACS*, and *MT-ATP6* (Figure 4e). These genes are downregulated in the FRDA iNs (except *SACS* and *MT-ATP6* that are upregulated). Genes belonging to these processes and pathways were also differentially expressed when FRDA cells were compared to an unrelated control. Furthermore, they were restored to control levels when FRDA-derived

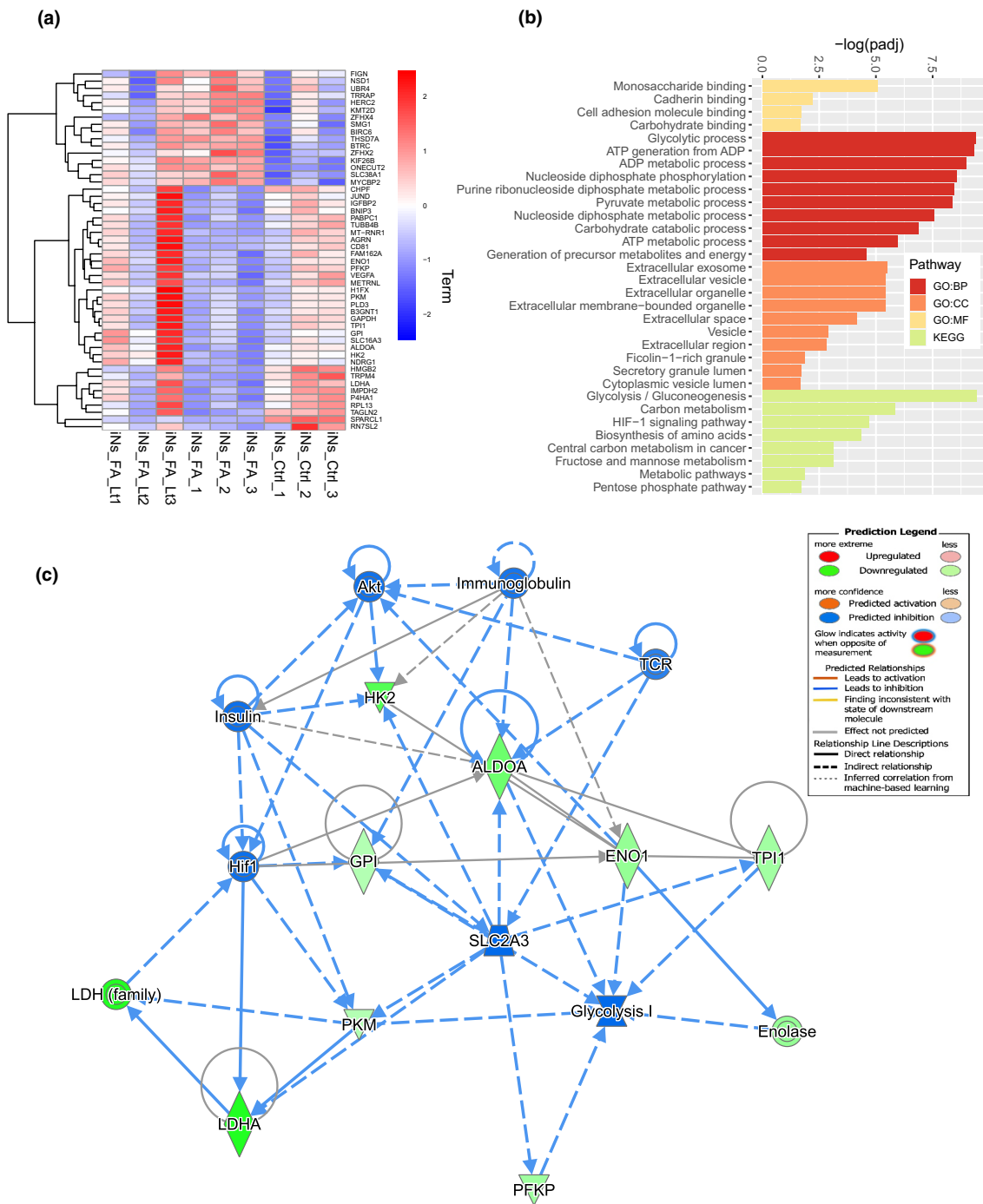


**FIGURE 6** Differentially expressed genes in FRDA vs. control iNs corrected by frataxin transduction. (a) Heatmap illustrating the expression of DE genes in FRDA and control iNs that are restored to control level when transduced with FXN lentivirus. Three independent replicates are shown per group. (b) Enrichment analysis of corrected genes using g:Profiler. We included results from the gene ontology and KEGG databases. (c) Ingenuity pathway analysis (IPA) of the genes from the most enriched pathway of corrected iNs (glycolysis/ gluconeogenesis). IPA generated a network diagram with the most probable connections to each other and to additional genes in the IPA knowledge base. \*FA means FRDA.

iNs were supplemented with frataxin. The differentially expressed genes from the most enriched pathways in corrected iNs were *GPI*, *HK2*, *TPI1*, *ALDOA*, *ENO1*, *LDHA*, *PFKP*, and *PKM* (Figure 6b). Interestingly all these genes were downregulated in FRDA-derived iNs.

*GPI* encodes for a member of the glucose phosphate isomerase protein family. This protein performs distinct functions; it acts as a glycolytic enzyme in the cytoplasm. However, extracellularly, it operates as a neurotrophic factor promoting survival of motor and sensory neurons'

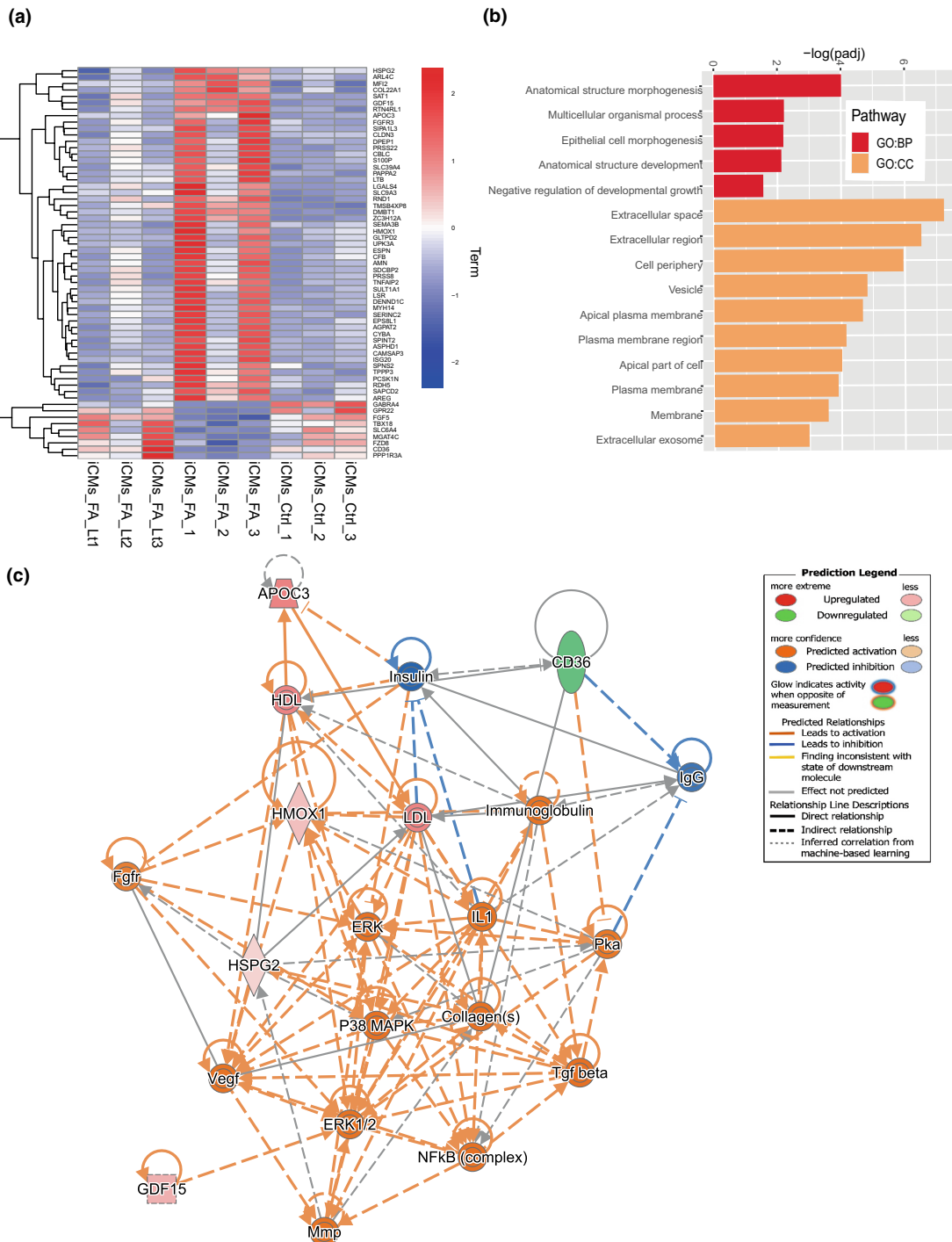


**FIGURE 7** Differentially expressed genes in FRDA vs. control iCMs corrected by frataxin transduction. (a) Heatmap illustrating the expression of DE genes in FRDA and control iCMs that are restored to control level when transduced with frataxin lentivirus. Three independent replicates are shown per group. (b) Enrichment analysis of corrected genes using g:Profiler. We obtained results from the gene ontology database. (c) Ingenuity pathway analysis (IPA) of the genes from the most enriched pathway of corrected iCMs (extracellular space). IPA generated a network diagram with the most probable connections to each other and to additional genes in the IPA knowledge base. \*FA means FRDA.

(Faik et al., 1988) the most affected neurons in FRDA. Although this gene has not been associated with FRDA, defects in this gene are associated with neurological impairment (Romagnoli et al., 2003). *HK2* catalyzes the first

essential step of glycolysis. It also plays a role in maintaining the integrity of the outer mitochondrial membrane by preventing the release of apoptogenic proteins from the intermembrane space and consequent cell death (Chiara

et al., 2008). Loss of mitochondrial membrane potential and mitochondrial defects are phenotypes observed in FRDA cells and is a sign of bioenergetic stress (Codazzi et al., 2016; Hick et al., 2013; Lee et al., 2016). *TPII* encodes a metabolic enzyme important in glycolysis and gluconeogenesis. Deficiency of this enzyme causes anemia, movement problems, increased susceptibility to infection, and muscle weakness (Orosz et al., 2006).

Other downregulated genes that are part of energy metabolism include *ALDOA*, *ENO1*, *LDHA*, *PFKP*, and *PKM*. Cells with high energy demands, such as nerve cells and heart muscle cells, are susceptible to cell death due to reduced energy caused by impaired glycolysis, and these are the most affected cells in FRDA. *ENO1* can associate with mitochondrial membrane, and it is essential for membrane stability (Didiasova et al., 2019). *LDHA* deficiency is associated with neuronal damage in Alzheimer's Disease (Zhang et al., 2018). The IPA shows how these genes are connected in a signaling network (Figure 6c), demonstrating the possibility that frataxin is involved in glycolysis and other neuropathy-associated genes in FRDA.

Previous studies in iPSC-derived iNs from FRDA have shown lower ATP levels, decreased aconitase activity, and reduced mitochondrial membrane potential (Codazzi et al., 2016; Hick et al., 2013; Li et al., 2015). Therefore, these phenotypes are consistent with our findings. Interestingly, when compared to another transcriptional profile study in FRDA iPSC-derived iNs, the only shared process is the one related to extracellular matrix (Lai et al., 2019). This discrepancy could reflect the variability between patients, controls, and techniques to over-express frataxin. In the study by Lai et al, a combination of HDAC inhibition and gene editing was used with iNs. These methods focused on the GAA expansion instead of just correcting the *FXN* level.

Restoring frataxin in iCMs led to changes in 417 genes, which are related to processes and components of the extracellular matrix. Pathways analyses indicated that the most significant enrichment is for the extracellular matrix (Figure 5e). Our FRDA subject had mild cardiac symptoms, suggesting that cardiac involvement was in its early phase.

Genes differentially expressed in a frataxin-dependent manner in FRDA-iCMs were compared with control iCMs were enriched in extracellular matrix and the plasma membrane maintenance pathways. Potentially relevant genes include *GDF15*, *HMOX1*, and *HSPG2*, which were upregulated in FRDA iCMs. *GDF15* encodes a secreted ligand of TGF-beta (also known as Macrophage inhibitory cytokine-1). Several studies have associated *GDF15* and cardiac fibrosis. In addition to this, *GDF15* also increases in response to cellular and mitochondrial dysfunction. It acts as an inflammatory marker and is a player in the

pathogenesis of cardiovascular diseases, metabolic disorders, and neurodegenerative processes (Foley et al., 2009; Kempf & Wollert, 2009; Rochette et al., 2021; Yatsuga et al., 2015). This correlation suggests that *GDF15* may have potential as a serum biomarker for FRDA-associated heart disease (Kempf et al., 2007).

*HMOX1* encodes for the heme oxygenase 1 enzyme, which mediates the first step of heme catabolism. *HMOX* upregulation has been implicated in increased ferroptosis in diabetic atherosclerosis (Meng et al., 2021). Frataxin is involved in iron regulation and heme synthesis with ferroptosis as a newly proposed mechanism in FRDA (Turchi et al., 2020), and 10%–30% of FRDA patients develop diabetes (Cnop et al., 2012; Gucev et al., 2009). *HSPG2* gene encodes for perlecan, a heparin sulfate proteoglycan found in the extracellular matrix. Perlecan has been implicated in various pathologies associated with extracellular matrix remodeling, including diabetes, cardiovascular disease, and Alzheimer's disease (Martinez et al., 2018). The IPA shows how these genes are connected in a signaling network to other differentially expressed genes in the IPA knowledge base (Figure 7c). This illustrates the possibilities of frataxin interactions in cardiomyocytes involved in remodeling the extracellular matrix in FRDA.

When comparing the differentially expressed genes of FRDA iPSC-derived iCMs from this study with another study in iCMs derived from an FRDA patient (Li et al., 2019), we found that the shared dysregulated genes belong to processes related to the extracellular matrix. Some of the processes are supramolecular collagen fibril organization, collagen fibril organization, extracellular space, and extracellular matrix (Table S4). This further supports the evidence that extracellular matrix remodeling plays a role in developing cardiac disease in FRDA and that frataxin dysregulation is involved in this process.

The goal of our study was to directly evaluate the role of the frataxin-deficiency independent of the GAA expansion or effects of drugs. By doing this, we identified key interactions of a frataxin network that may contribute to FRDA pathogenesis. Genes involved in glycolysis seem to have an essential role in the neurological aspect of FRDA, whereas genes related to the extracellular matrix are fundamental for the development of cardiac disease. This difference between iNs and iCMs may offer insights into unique effects and susceptibilities of the neuros and the heart in FRDA. The heart and neurons differ significantly in their energy sources and susceptibility to nutrient deprivation. In the healthy human heart >95% of the ATP is produced from oxidative phosphorylation in the mitochondria. The preferred substrates are fatty acids accounting for 70%–90% of ATP. Approximately 10%–25% of myocardia ATP comes from oxidation of glucose, lactate, amino acids, and ketone bodies. Glycolysis and

the citric acid cycle account for about 5% of myocardial ATP (Stanley et al., 2005; Taegtmeyer, 1994). Most cardiac disease states (e.g., ischemia, heart failure, hypertrophy) exhibit reduced myocardial energy production with a shift away from fatty acids-oxidation towards more glucose-dependence (Neubauer, 2007). Central neurons rely almost exclusively on glycolysis with full oxidation of glycolytic products by oxidative phosphorylation in the mitochondria (Dalsgaard, 2006; Yellen, 2018). Thus, the perturbation of glycolytic pathway gene expression in FRDA neurons may explain why the earliest manifestation of the disease is usually neurological while cardiac pathology is later and more variable.

#### 4.1 | Limitations of this study

It is interesting to observe that few genes and pathways overlap when comparing this study to other RNA-seq studies in FRDA-relevant cells. This could reflect the different techniques used to generate iNs and iCMs, to up-regulate frataxin, the patient-to-patient variability, as well as our study limitations. We did not use an isogenic cell line as a control, and the results are from one patient. Therefore, the generation of isogenic cell lines and studies with multiple patients is vital in resolving which genes are truly associated with the disease. We also did not observe any physiologically relevant phenotype in the FRDA cells. Therefore, the ability to mature the iPSC-derived cells to generate phenotypes that could be corrected with frataxin replacement will be critical in obtaining the complete picture of how FRDA develops.

#### AUTHOR CONTRIBUTIONS

Project conception and design (TVM, MBA), recruitment of FRDA subjects (TZ, AP), clinical phenotyping (TZ, AP), acquisition of data (MBA, AB, JY), analysis and interpretation of data (MBA, AB, MAA, TVM), and writing and editing of manuscript (MBA, AB, JY, MAA, TZ, AP, TVM).

#### ACKNOWLEDGMENTS


We thank the patient for donating his blood sample for this research.

#### FUNDING INFORMATION

This work was supported by the USF-Preeminence Fund.

#### ORCID

Mariana B. Angulo  <https://orcid.org/0000-0002-1982-8102>

Thomas V. McDonald  <https://orcid.org/0000-0002-6075-0888>

#### REFERENCES

- Adamec, J., Rusnak, F., Owen, W. G., Naylor, S., Benson, L. M., Gacy, A. M., & Isaya, G. (2000). Iron-dependent self-assembly of recombinant yeast frataxin: Implications for Friedreich ataxia. *American Journal of Human Genetics*, 67(3), 549–562. <https://doi.org/10.1086/303056>
- Adinolfi, S., Iannuzzi, C., Prischi, F., Pastore, C., Iametti, S., Martin, S. R., Bonomi, F., & Pastore, A. (2009). Bacterial frataxin CyaY is the gatekeeper of iron-sulfur cluster formation catalyzed by IscS. *Nature Structural & Molecular Biology*, 16(4), 390–396. <https://doi.org/10.1038/nsmb.1579>
- Al-Mahdawi, S., Pinto, R. M., Ismail, O., Varshney, D., Lymperi, S., Sandi, C., Trabzuni, D., & Pook, M. (2008). The Friedreich ataxia GAA repeat expansion mutation induces comparable epigenetic changes in human and transgenic mouse brain and heart tissues. *Human Molecular Genetics*, 17(5), 735–746. <https://doi.org/10.1093/hmg/ddm346>
- Angulo, M. B., Yang, J., Argenziano, M. A., Bertalovitz, A. C., Beidokhti, M. N., & McDonald, T. V. (2021). Generation of a Friedreich's ataxia patient-derived iPSC line USFi001-a. *Stem Cell Research*, 54, 102399. <https://doi.org/10.1016/j.scr.2021.102399>
- Aranca, T. V., Jones, T. M., Shaw, J. D., Staffetti, J. S., Ashizawa, T., Kuo, S. H., Fogel, B. L., Wilmot, G. R., Perlman, S. L., Onyike, C. U., Ying, S. H., & Zesiewicz, T. A. (2016). Emerging therapies in Friedreich's ataxia. *Neurodegenerative Disease Management*, 6(1), 49–65. <https://doi.org/10.2217/nmt.15.73>
- Becker, E. M., Greer, J. M., Ponka, P., & Richardson, D. R. (2002). Erythroid differentiation and protoporphyrin IX down-regulate frataxin expression in friend cells: Characterization of frataxin expression compared to molecules involved in iron metabolism and hemoglobinization. *Blood*, 99(10), 3813–3822. <https://doi.org/10.1182/blood.v99.10.3813>
- Belbellaa, B., Reutenauer, L., Messaddeq, N., Monassier, L., & Puccio, H. (2020). High levels of Frataxin overexpression Lead to mitochondrial and cardiac toxicity in mouse models. *Molecular Therapy-Methods & Clinical Development*, 19, 120–138. <https://doi.org/10.1016/j.omtm.2020.08.018>
- Bolnches-Amoros, A., Molla, B., Pla-Martin, D., Palau, F., & Gonzalez-Cabo, P. (2014). Mitochondrial dysfunction induced by frataxin deficiency is associated with cellular senescence and abnormal calcium metabolism. *Frontiers in Cellular Neuroscience*, 8, 124. <https://doi.org/10.3389/fncel.2014.00124>
- Campuzano, V., Montermini, L., Lutz, Y., Cova, L., Hindelang, C., Jiralerspong, S., Trottier, Y., Kish, S. J., Faucheux, B., Trouillas, P., Authier, F. J., Dürr, A., Mandel, J. L., Vescovi, A., Pandolfo, M., & Koenig, M. (1997). Frataxin is reduced in Friedreich ataxia patients and is associated with mitochondrial membranes. *Human Molecular Genetics*, 6(11), 1771–1780. <https://doi.org/10.1093/hmg/6.11.1771>
- Campuzano, V., Montermini, L., Molto, M. D., Pianese, L., Cossee, M., Cavalcanti, F., Monros, E., Rodius, F., Duclos, F., Monticelli, A., Zara, F., Cañizares, J., Koutnikova, H., Bidichandani, S. I., Gellera, C., Brice, A., Trouillas, P., De Michele, G., Filla, A., & Pandolfo, M. (1996). Friedreich's ataxia: Autosomal recessive disease caused by an intronic GAA triplet repeat expansion. *Science*, 271(5254), 1423–1427. <https://doi.org/10.1126/science.271.5254.1423>
- Castaldo, I., Pinelli, M., Monticelli, A., Acquaviva, F., Giacchetti, M., Filla, A., Sacchetti, S., Keller, S., Avvedimento, V. E.,



- Chiariotti, L., & Coccozza, S. (2008). DNA methylation in intron 1 of the frataxin gene is related to GAA repeat length and age of onset in Friedreich ataxia patients. *Journal of Medical Genetics*, *45*(12), 808–812. <https://doi.org/10.1136/jmg.2008.058594>
- Chandran, V., Gao, K., Swarup, V., Versano, R., Dong, H., Jordan, M. C., & Geschwind, D. H. (2017). Inducible and reversible phenotypes in a novel mouse model of Friedreich's ataxia. *eLife*, *6*, e30054. <https://doi.org/10.7554/eLife.30054>
- Chiara, F., Castellaro, D., Marin, O., Petronilli, V., Brusilow, W. S., Juhaszova, M., Sollott, S. J., Forte, M., Bernardi, P., & Rasola, A. (2008). Hexokinase II detachment from mitochondria triggers apoptosis through the permeability transition pore independent of voltage-dependent anion channels. *PLoS One*, *3*(3), e1852. <https://doi.org/10.1371/journal.pone.0001852>
- Cnop, M., Igoillo-Esteve, M., Rai, M., Begu, A., Serroukh, Y., Depondt, C., Musuaya, A. E., Marhfour, I., Ladrière, L., Moles Lopez, X., Lefkaditis, D., Moore, F., Brion, J.-P., Cooper, J. M., Schapira, A. H. V., Clark, A., Koeppen, A. H., Marchetti, P., Pandolfo, M., ... Fery, F. (2012). Central role and mechanisms of beta-cell dysfunction and death in friedreich ataxia-associated diabetes. *Annals of Neurology*, *72*(6), 971–982. <https://doi.org/10.1002/ana.23698>
- Codazzi, F., Hu, A., Rai, M., Donatello, S., Salerno Scarzella, F., Mangiameli, E., Pelizzoni, I., Grohovaz, F., & Pandolfo, M. (2016). Friedreich ataxia-induced pluripotent stem cell-derived neurons show a cellular phenotype that is corrected by a benzamide HDAC inhibitor. *Human Molecular Genetics*, *25*(22), 4847–4855. <https://doi.org/10.1093/hmg/ddw308>
- Cook, A., & Giunti, P. (2017). Friedreich's ataxia: Clinical features, pathogenesis and management. *British Medical Bulletin*, *124*(1), 19–30. <https://doi.org/10.1093/bmb/ldx034>
- Cossee, M., Schmitt, M., Campuzano, V., Reutenauer, L., Moutou, C., Mandel, J. L., & Koenig, M. (1997). Evolution of the Friedreich's ataxia trinucleotide repeat expansion: Founder effect and premutations. *Proceedings of the National Academy of Sciences of the United States of America*, *94*(14), 7452–7457. <https://doi.org/10.1073/pnas.94.14.7452>
- Dalsgaard, M. K. (2006). Fuelling cerebral activity in exercising man. *Journal of Cerebral Blood Flow and Metabolism*, *26*(6), 731–750. <https://doi.org/10.1038/sj.jcbfm.9600256>
- De Biase, I., Rasmussen, A., Monticelli, A., Al-Mahdawi, S., Pook, M., Coccozza, S., & Bidichandani, S. I. (2007). Somatic instability of the expanded GAA triplet-repeat sequence in Friedreich ataxia progresses throughout life. *Genomics*, *90*(1), 1–5. <https://doi.org/10.1016/j.ygeno.2007.04.001>
- Delatycki, M. B., & Bidichandani, S. I. (2019). Friedreich ataxia-pathogenesis and implications for therapies. *Neurobiology of Disease*, *132*, 104606. <https://doi.org/10.1016/j.nbd.2019.104606>
- Delatycki, M. B., Williamson, R., & Forrest, S. M. (2000). Friedreich ataxia: An overview. *Journal of Medical Genetics*, *37*(1), 1–8. <https://doi.org/10.1136/jmg.37.1.1>
- Didiasova, M., Schaefer, L., & Wygrecka, M. (2019). When place matters: Shuttling of Enolase-1 across cellular compartments. *Frontiers in Cell and Development Biology*, *7*, 61. <https://doi.org/10.3389/fcell.2019.00061>
- Faik, P., Walker, J. I., Redmill, A. A., & Morgan, M. J. (1988). Mouse glucose-6-phosphate isomerase and neuroleukin have identical 3' sequences. *Nature*, *332*(6163), 455–457. <https://doi.org/10.1038/332455a0>
- Finocchiaro, G., Baio, G., Micossi, P., Pozza, G., & di Donato, S. (1988). Glucose metabolism alterations in Friedreich's ataxia. *Neurology*, *38*(8), 1292–1296. <https://doi.org/10.1212/wnl.38.8.1292>
- Foley, P. W., Stegemann, B., Ng, K., Ramachandran, S., Proudler, A., Frenneaux, M. P., Ng, L. L., & Leyva, F. (2009). Growth differentiation factor-15 predicts mortality and morbidity after cardiac resynchronization therapy. *European Heart Journal*, *30*(22), 2749–2757. <https://doi.org/10.1093/eurheartj/ehp300>
- Gucev, Z., Tasic, V., Jancevska, A., Popjordanova, N., Koceva, S., Kuturec, M., & Sabolic, V. (2009). Friedreich ataxia (FA) associated with diabetes mellitus type 1 and hyperthrophic cardiomyopathy. *Bosnian Journal of Basic Medical Sciences*, *9*(2), 107–110. <https://doi.org/10.17305/bjbm.2009.2828>
- Gunal, N., Saraclar, M., Ozkutlu, S., Senocak, F., Topaloglu, H., & Karaaslan, S. (1996). Heart disease in Friedreich's ataxia: A clinical and echocardiographic study. *Acta Paediatrica Japonica*, *38*(4), 308–311. <https://doi.org/10.1111/j.1442-200x.1996.tb03496.x>
- Hanson, E., Sheldon, M., Pacheco, B., Alkubeysi, M., & Raizada, V. (2019). Heart disease in Friedreich's ataxia. *World Journal of Cardiology*, *11*(1), 1–12. <https://doi.org/10.4330/wjc.v11.i1.1>
- Harding, A. E., & Hewer, R. L. (1983). The heart disease of Friedreich's ataxia: A clinical and electrocardiographic study of 115 patients, with an analysis of serial electrocardiographic changes in 30 cases. *The Quarterly Journal of Medicine*, *52*(208), 489–502. <https://www.ncbi.nlm.nih.gov/pubmed/6228949>
- Heidari, M. M., Houshmand, M., Hosseinkhani, S., Nafissi, S., & Khatami, M. (2009). Complex I and ATP content deficiency in lymphocytes from Friedreich's ataxia. *The Canadian Journal of Neurological Sciences*, *36*(1), 26–31. <https://doi.org/10.1017/s0317167100006260>
- Hick, A., Wattenhofer-Donze, M., Chintawar, S., Tropel, P., Simard, J. P., Vaucamps, N., Gall, D., Lambot, L., André, C., Reutenauer, L., Rai, M., Teletin, M., Messaddeq, N., Schiffmann, S. N., Viville, S., Pearson, C. E., Pandolfo, M., & Puccio, H. (2013). Neurons and cardiomyocytes derived from induced pluripotent stem cells as a model for mitochondrial defects in Friedreich's ataxia. *Disease Models & Mechanisms*, *6*(3), 608–621. <https://doi.org/10.1242/dmm.010900>
- Huichalaf, C., Perfitt, T. L., Kuperman, A., Gooch, R., Kovi, R. C., Brenneman, K. A., Chen, X., Hirehallur-Shanthappa, D., Ma, T., Assaf, B. T., Pardo, I., Franks, T., Monarski, L., Cheng, T.-W., Le, K., Su, C., Somanathan, S., Whiteley, L. O., Bulawa, C., ... Martelli, A. (2022). In vivo overexpression of frataxin causes toxicity mediated by iron-sulfur cluster deficiency. *Molecular Therapy. Methods & Clinical Development*, *24*, 367–378. <https://doi.org/10.1016/j.omtm.2022.02.002>
- Isaacs, C. J., Brigatti, K. W., Kucheruk, O., Ratcliffe, S., Sciascia, T., McCormack, S. E., Willi, S. M., & Lynch, D. R. (2016). Effects of genetic severity on glucose homeostasis in Friedreich ataxia. *Muscle & Nerve*, *54*(5), 887–894. <https://doi.org/10.1002/mus.25136>
- Kawai, C., Kato, S., Takashima, M., Fujiwara, H., & Haebara, H. (2000). Heart disease in Friedreich's ataxia: Observation of a case for half a century. *Japanese Circulation Journal*, *64*(3), 229–236. <https://doi.org/10.1253/jcj.64.229>
- Keita, M., McIntyre, K., Rodden, L. N., Schadt, K., & Lynch, D. R. (2022). Friedreich ataxia: Clinical features and new developments. *Neurodegenerative Disease Management*, *12*, 267–283. <https://doi.org/10.2217/nmt-2022-0011>
- Kempf, T., von Haehling, S., Peter, T., Allhoff, T., Cicoira, M., Doehner, W., Ponikowski, P., Filippatos, G. S., Rozenytr, P., Drexler,

- H., Anker, S. D., & Wollert, K. C. (2007). Prognostic utility of growth differentiation factor-15 in patients with chronic heart failure. *Journal of the American College of Cardiology*, 50(11), 1054–1060. <https://doi.org/10.1016/j.jacc.2007.04.091>
- Kempf, T., & Wollert, K. C. (2009). Growth-differentiation factor-15 in heart failure. *Heart Failure Clinics*, 5(4), 537–547. <https://doi.org/10.1016/j.hfc.2009.04.006>
- Koepfen, A. H., & Mazurkiewicz, J. E. (2013). Friedreich ataxia: Neuropathology revised. *Journal of Neuropathology and Experimental Neurology*, 72(2), 78–90. <https://doi.org/10.1097/NEN.0b013e31827e5762>
- Koepfen, A. H., Ramirez, R. L., Becker, A. B., Bjork, S. T., Levi, S., Santambrogio, P., Parsons, P. J., Kruger, P. C., Yang, K. X., Feustel, P. J., & Mazurkiewicz, J. E. (2015). The pathogenesis of cardiomyopathy in Friedreich ataxia. *PLoS One*, 10(3), e0116396. <https://doi.org/10.1371/journal.pone.0116396>
- Koutnikova, H., Campuzano, V., Foury, F., Dolle, P., Cazzalini, O., & Koenig, M. (1997). Studies of human, mouse and yeast homologues indicate a mitochondrial function for frataxin. *Nature Genetics*, 16(4), 345–351. <https://doi.org/10.1038/ng0897-345>
- Lai, J. I., Nachun, D., Petrosyan, L., Throesch, B., Campau, E., Gao, F., Baldwin, K. K., Coppola, G., Gottesfeld, J. M., & Soragni, E. (2019). Transcriptional profiling of isogenic Friedreich ataxia neurons and effect of an HDAC inhibitor on disease signatures. *The Journal of Biological Chemistry*, 294(6), 1846–1859. <https://doi.org/10.1074/jbc.RA118.006515>
- Lee, Y. K., Lau, Y. M., Ng, K. M., Lai, W. H., Ho, S. L., Tse, H. F., Siu, C. W., & Ho, P. W. (2016). Efficient attenuation of Friedreich's ataxia (FRDA) cardiomyopathy by modulation of iron homeostasis-human induced pluripotent stem cell (hiPSC) as a drug screening platform for FRDA. *International Journal of Cardiology*, 203, 964–971. <https://doi.org/10.1016/j.ijcard.2015.11.101>
- Li, J., Rozwadowska, N., Clark, A., Fil, D., Napierala, J. S., & Napierala, M. (2019). Excision of the expanded GAA repeats corrects cardiomyopathy phenotypes of iPSC-derived Friedreich's ataxia cardiomyocytes. *Stem Cell Research*, 40, 101529. <https://doi.org/10.1016/j.scr.2019.101529>
- Li, Y., Polak, U., Bhalla, A. D., Rozwadowska, N., Butler, J. S., Lynch, D. R., Dent, S. Y., & Napierala, M. (2015). Excision of expanded GAA repeats alleviates the molecular phenotype of Friedreich's ataxia. *Molecular Therapy*, 23(6), 1055–1065. <https://doi.org/10.1038/mt.2015.41>
- Lim, F., Palomo, G. M., Mauritz, C., Gimenez-Cassina, A., Illana, B., Wandosell, F., & Diaz-Nido, J. (2007). Functional recovery in a Friedreich's ataxia mouse model by frataxin gene transfer using an HSV-1 amplicon vector. *Molecular Therapy*, 15(6), 1072–1078. <https://doi.org/10.1038/sj.mt.6300143>
- Livak, K. J., & Schmittgen, T. D. (2001). Analysis of relative gene expression data using real-time quantitative PCR and the 2(-Delta Delta C[T]) method. *Methods*, 25(4), 402–408. <https://doi.org/10.1006/meth.2001.1262>
- Lodi, R., Cooper, J. M., Bradley, J. L., Manners, D., Styles, P., Taylor, D. J., & Schapira, A. H. (1999). Deficit of in vivo mitochondrial ATP production in patients with Friedreich ataxia. *Proceedings of the National Academy of Sciences of the United States of America*, 96(20), 11492–11495. <https://doi.org/10.1073/pnas.96.20.11492>
- Long, A., Napierala, J. S., Polak, U., Hauser, L., Koepfen, A. H., Lynch, D. R., & Napierala, M. (2017). Somatic instability of the expanded GAA repeats in Friedreich's ataxia. *PLoS One*, 12(12), e0189990. <https://doi.org/10.1371/journal.pone.0189990>
- Martinez, J. R., Dhawan, A., & Farach-Carson, M. C. (2018). Modular proteoglycan Perlecan/HSPG2: Mutations, phenotypes, and functions. *Genes (Basel)*, 9(11), 556. <https://doi.org/10.3390/genes9110556>
- Meng, Z., Liang, H., Zhao, J., Gao, J., Liu, C., Ma, X., Liu, J., Liang, B., Jiao, X., Cao, J., & Wang, Y. (2021). HMOX1 upregulation promotes ferroptosis in diabetic atherosclerosis. *Life Sciences*, 284, 119935. <https://doi.org/10.1016/j.lfs.2021.119935>
- Neubauer, S. (2007). The failing heart—An engine out of fuel. *The New England Journal of Medicine*, 356(11), 1140–1151. <https://doi.org/10.1056/NEJMra063052>
- Orosz, F., Olah, J., & Ovadi, J. (2006). Triosephosphate isomerase deficiency: Facts and doubts. *IUBMB Life*, 58(12), 703–715. <https://doi.org/10.1080/15216540601115960>
- Pousset, F., Legrand, L., Monin, M. L., Ewencyk, C., Charles, P., Komajda, M., Brice, A., Pandolfo, M., Isnard, R., du Montcel, S. T., & Durr, A. (2015). A 22-year follow-up study of Long-term cardiac outcome and predictors of survival in Friedreich ataxia. *JAMA Neurology*, 72(11), 1334–1341. <https://doi.org/10.1001/jamaneurol.2015.1855>
- Qin, J. Y., Zhang, L., Clift, K. L., Hulur, I., Xiang, A. P., Ren, B. Z., & Lahn, B. T. (2010). Systematic comparison of constitutive promoters and the doxycycline-inducible promoter. *PLoS One*, 5(5), e10611. <https://doi.org/10.1371/journal.pone.0010611>
- Rochette, L., Dogon, G., Zeller, M., Cottin, Y., & Vergely, C. (2021). GDF15 and cardiac cells: Current concepts and new insights. *International Journal of Molecular Sciences*, 22(16), 8889. <https://doi.org/10.3390/ijms22168889>
- Romagnoli, A., Oliverio, S., Evangelisti, C., Iannicola, C., Ippolito, G., & Piacentini, M. (2003). Neuroleukin inhibition sensitises neuronal cells to caspase-dependent apoptosis. *Biochemical and Biophysical Research Communications*, 302(3), 448–453. [https://doi.org/10.1016/s0006-291x\(03\)00188-8](https://doi.org/10.1016/s0006-291x(03)00188-8)
- Sacca, F., Puorro, G., Antenora, A., Marsili, A., Denaro, A., Piro, R., Sorrentino, P., Pane, C., Tessa, A., Brescia Morra, V., Coccozza, S., De Michele, G., Santorelli, F. M., & Filla, A. (2011). A combined nucleic acid and protein analysis in Friedreich ataxia: Implications for diagnosis, pathogenesis and clinical trial design. *PLoS One*, 6(3), e17627. <https://doi.org/10.1371/journal.pone.0017627>
- Stanley, W. C., Recchia, F. A., & Lopaschuk, G. D. (2005). Myocardial substrate metabolism in the normal and failing heart. *Physiological Reviews*, 85(3), 1093–1129. <https://doi.org/10.1152/physrev.00006.2004>
- Taegtmeier, H. (1994). Energy metabolism of the heart: From basic concepts to clinical applications. *Current Problems in Cardiology*, 19(2), 59–113. [https://doi.org/10.1016/0146-2806\(94\)90008-6](https://doi.org/10.1016/0146-2806(94)90008-6)
- Turchi, R., Faraonio, R., Lettieri-Barbato, D., & Aquilano, K. (2020). An overview of the Ferroptosis hallmarks in Friedreich's ataxia. *Biomolecules*, 10(11), 1489. <https://doi.org/10.3390/biom10111489>
- Vannocci, T., Notario Manzano, R., Beccalli, O., Bettegazzi, B., Grohovaz, F., Cinque, G., De Riso, A., Quaroni, L., Codazzi, F., & Pastore, A. (2018). Adding a temporal dimension to the study of Friedreich's ataxia: The effect of frataxin overexpression in a human cell model. *Disease Models & Mechanisms*, 11(6), dmm032706. <https://doi.org/10.1242/dmm.032706>

- Worth, A. J., Basu, S. S., Deutsch, E. C., Hwang, W. T., Snyder, N. W., Lynch, D. R., & Blair, I. A. (2015). Stable isotopes and LC-MS for monitoring metabolic disturbances in Friedreich's ataxia platelets. *Bioanalysis*, 7(15), 1843–1855. <https://doi.org/10.4155/bio.15.118>
- Yatsuga, S., Fujita, Y., Ishii, A., Fukumoto, Y., Arahata, H., Kakuma, T., Kojima, T., Ito, M., Tanaka, M., Saiki, R., & Koga, Y. (2015). Growth differentiation factor 15 as a useful biomarker for mitochondrial disorders. *Annals of Neurology*, 78(5), 814–823. <https://doi.org/10.1002/ana.24506>
- Yellen, G. (2018). Fueling thought: Management of glycolysis and oxidative phosphorylation in neuronal metabolism. *The Journal of Cell Biology*, 217(7), 2235–2246. <https://doi.org/10.1083/jcb.201803152>
- Yoon, T., & Cowan, J. A. (2003). Iron-sulfur cluster biosynthesis. Characterization of frataxin as an iron donor for assembly of [2Fe-2S] clusters in ISU-type proteins. *Journal of the American Chemical Society*, 125(20), 6078–6084. <https://doi.org/10.1021/ja027967i>
- Yoon, T., & Cowan, J. A. (2004). Frataxin-mediated iron delivery to ferrochelatase in the final step of heme biosynthesis. *The Journal of Biological Chemistry*, 279(25), 25943–25946. <https://doi.org/10.1074/jbc.C400107200>
- Zesiewicz, T. A., Hancock, J., Ghanekar, S. D., Kuo, S. H., Dohse, C. A., & Vega, J. (2020). Emerging therapies in Friedreich's ataxia. *Expert Review of Neurotherapeutics*, 20(12), 1215–1228. <https://doi.org/10.1080/14737175.2020.1821654>
- Zhang, M., Cheng, X., Dang, R., Zhang, W., Zhang, J., & Yao, Z. (2018). Lactate deficit in an Alzheimer disease mouse model: The relationship with neuronal damage. *Journal of Neuropathology and Experimental Neurology*, 77(12), 1163–1176. <https://doi.org/10.1093/jnen/nly102>

## SUPPORTING INFORMATION

Additional supporting information can be found online in the Supporting Information section at the end of this article.

**How to cite this article:** Angulo, M. B., Bertalovitz, A., Argenziano, M. A., Yang, J., Patel, A., Zesiewicz, T., & McDonald, T. V. (2023). Frataxin deficiency alters gene expression in Friedreich ataxia derived iPSC-neurons and cardiomyocytes. *Molecular Genetics & Genomic Medicine*, 11, e2093. <https://doi.org/10.1002/mgg3.2093>